Available online at www.sciencedirect.com
ScienceDirect
Journal of Nuclear Materials 377 (2008) 162–173
journal of nuclear materials
www.elsevier.com/locate/jnucmat

Cavitation damage experiments for mercury spallation targets at the LANSCE – WNR in 2005

B. Riemer [a,*], J. Haines [a], M. Wendel [a], G. Bauer [b], M. Futakawa [c], S. Hasegawa [c], H. Kogawa [c]

[a] *Spallation Neutron Source/ORNL[1], P.O. Box 2008, Building 8600, MS 6466, Oak Ridge, TN 37831, USA*
[b] *Forschungszentrum Jülich, Leo-Brandt-Strasse, 52425 Jülich, North Rhine-Westphalia, Germany*
[c] *Center for Proton Accelerator Facilities, JAEA, Tokai-mura, Ibaraki-ken 319-1195, Japan*

Abstract

In-beam experiments investigating cavitation damage in short pulse mercury spallation targets were performed at the Los Alamos Neutron Science Center – Weapons Neutron Research (LANSCE – WNR) facility in 2005. Two main areas were investigated. First, damage dependence on three mercury conditions – stagnant, flowing, and flowing with bubble injection – was investigated by employing a small mercury target loop with replaceable damage test specimens. One hundred beam pulses were passed through the loop mercury and specimen pair for each test condition. Damage with flowing mercury ($V = 0.4$ m/s) was less than half that which was incurred with stagnant mercury. Gas bubble injection added into the flow further reduced damage to about one-fourth that of stagnant mercury. Acoustic emissions from cavitation bubble collapse were concurrently measured on the exterior of the loop using a laser Doppler vibrometer and were correlated to the observed damage. The second area of experimentation was erosion rate dependence on proton beam intensity. Prior research had indicated that incubation-phase cavitation erosion rate is strongly dependent on beam intensity, by a power law with the exponent perhaps as large as 4. The 2005 results are inconsistent with earlier in-beam test results and do not support the power law dependence. This paper will provide a detailed description of the experiment, present results and discuss the findings.
Published by Elsevier B.V.

1. Introduction

The US Spallation Neutron Source (SNS) and the Japanese Spallation Neutron Source (JSNS) both use short proton beam pulses (<1 μs) on mercury targets to produce neutrons [1–3]. Roughly one cubic meter per minute of mercury is circulated through a stainless steel target vessel that – for both facilities – will have to be periodically replaced because of radiation damage. However, the phenomena of beam induced cavitation damage might limit the useful life of the target vessel more severely than radiation damage [4–6]. Collaborative research and development is being conducted find ways to mitigate the damage so that it is no more life limiting that radiation damage.

Small gas bubble injection is a technique that was being developed by the European Spallation Source (ESS) project as a means to reduce mercury target vessel strain due to large pressure pulses associated with short proton pulse and high power operation. A population of small bubbles of sufficient void fraction would, in theory, absorb and attenuate the pressure pulse [7,8] thus relieving the load on the target vessel. Small bubbles have the ability to respond quickly to the rapid beam induced pressure; they also will tend to stay entrained in mercury flow while large bubbles are lost by buoyancy. Since cavitation damage is also driven by the pressure pulse, small bubble injection

* Corresponding author. Tel.: +1 865 574 6502.
E-mail address: riemerbw@ornl.gov (B. Riemer).
[1] ORNL/SNS is managed by UT-Battelle, LLC, for the US Department of Energy under contract DE-AC05-00OR22725.

0022-3115/$ - see front matter Published by Elsevier B.V.
doi:10.1016/j.jnucmat.2008.02.028

became one of the techniques being pursued by SNS and JSNS for cavitation damage mitigation.

Experiments conducted in June of 2005 at the LANSCE – WNR facility were the fourth in a sequence investigating cavitation damage in short pulse liquid metal spallation targets. Results from the earlier in-beam tests combined with off-line experiments have provided a body of data indicating cavitation erosion is a concern that may limit the target vessel lifetime and its power handling capacity (and hence, neutron intensity). The 2005 experiments had the primary goals to further investigate the small bubble damage mitigation technique and also to further evaluate damage dependence on incident proton intensity. Two types of mercury filled targets were employed for the tests.

A prior experiment for damage mitigation with small bubbles was part of a 2002 WNR test [4]. Cavitation damage in a mercury test target was reduced by approximately a factor of four with the introduction of bubbles. The result was encouraging but fell short of what is desired for a mercury spallation source target vessel (more than 10 times reduction). It was suspected that the achieved bubble population did not meet theoretical requirements, that is, a population of bubbles roughly 10 to 100 microns diameter and in total void fraction of about 0.001 should have been more effective in reducing damage. The 2002 experiment employed a tall, slender target design that simultaneously employed two different bubblers that relied on buoyancy to distribute the bubbles throughout the target. Unfortunately no credible measure of the established population was obtained during that experiment.

After the 2002 test result it was hoped that an improved test apparatus with more thorough pre-beam testing could achieve better damage mitigation and improve knowledge and experience with small bubble generation in mercury. Towards those ends a small loop was constructed to investigate the damage dependence on three mercury hydrodynamic conditions, namely, stagnant, flowing, and flowing with small helium bubbles injected into the mercury [9].

Rectangular-shaped targets with stagnant mercury had also been used in earlier WNR experiments for various reasons. One test sequence in 2002 investigated cavitation erosion rate dependence on equivalent SNS beam power based on proton intensity (expressed as protons/pulse/area). Those findings, in combination with off-line test results and theory, have indicated erosion rate to be proportional proton intensity raised to about the fourth power [4]. If true, the prospects for higher neutron source intensity could be challenging. It had been noted that the 2002 WNR experiment varied intensity by changing the number of protons per pulse while maintaining a fixed beam spot size and profile. A consequence was that total energy deposited in the targets varied between test conditions. A reasonable question to investigate is whether damage differences were due to the beam intensity changes or deposited energy. Therefore the 2005 test would change intensity by varying beam spot size while maintaining protons per pulse, and deposited energy.

2. Mercury loop experiment description

A small mercury loop was designed with several objectives based upon the use of small gas bubble injection for this 2005 experiment. Designated the in-beam bubble test loop, or IBBTL, its principal goal was to assess the change in proton pulse induced cavitation damage among three mercury hydrodynamic conditions, namely, static mercury, flowing mercury, and flowing mercury with small helium gas bubbles injected into the flow. Changes in-beam induced vessel strain between mercury conditions were also to be observed. Thirdly, velocity measurements of the loop exterior surface normal were to be made in order to evaluate and compare acoustic emissions associated with cavitation bubble collapse for each mercury condition. Such data has been shown to be useful for predicting relative damage in other cavitation experiments [10–12], but this would be the first attempted validation in a proton beam induced cavitation test.

Fig. 1 is a computer image of the IBBTL design showing its dimensions and Fig. 2 is a photo illustrating its major components. The loop was constructed of type 304 stain-

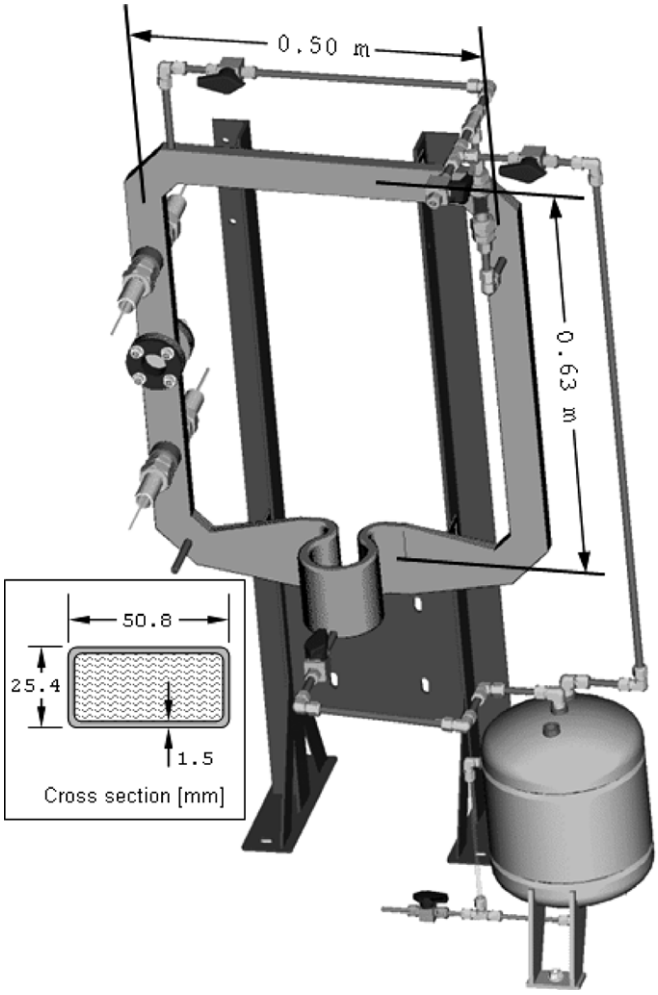

Fig. 1. Computer image of the IBBTL showing approximate dimensions.

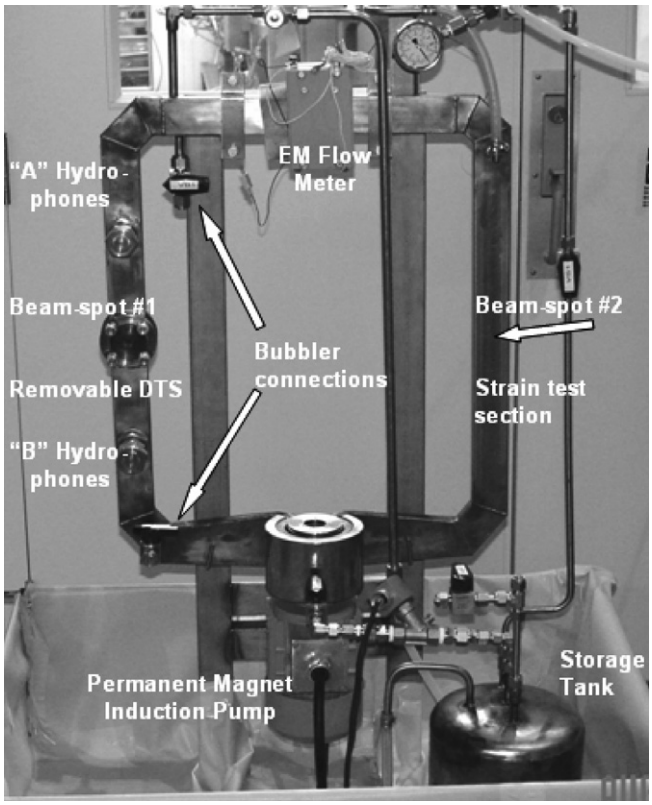

Fig. 2. The in-beam bubble test loop before instrumentation and secondary equipment were installed.

less steel tubing and is supported by a frame structure. The main loop flow was driven by a variable speed permanent magnet induction pump. During proton irradiation the entire apparatus was enclosed in a secondary container comprised of a stainless steel base and clear panel enclosure (not shown) to prevent uncontrolled liquid or vapor release. The loop was vented via mercury vapor absorbing filters; static operating pressure was limited to the mercury height. Major loop parameters are listed in Table 1. The basic loop structure, pump and secondary container were built by the Institute of Physics at the University of Latvia; substantial modifications and instrumentation were done at Oak Ridge National Laboratory (ORNL) before irradiation at the WNR.

Table 1
In-beam bubble test loop parameters

Main loop pressure	0–240 kPa absolute (excludes bubbler)
Steady-state operating temperature	<40 °C
Nominal Hg flow velocity in channel	0.4 m/s
Nominal flow rate	0.44 L/s
Nominal Hg pressure rise at main pump	1000 Pa
Hg inventory for IBBTL	4.5 L or 62 kg
Nominal bubbler Hg flow rate	0.02 L/s
Nominal pressure at bubbler pump	700–800 kPa (provides 500 kPa across bubbler jet)
Nominal bubbler He flow rate	140 mL/min

On the left vertical leg were removable damage test specimens (DTS) at the location designated beam spot #1 in Fig. 2. Above and below were hydrophone pair locations for acoustic measurement of the bubble population. The bubble generator used a bypass mercury flow driven by a peristaltic pump (Watson-Marlow Bredel SP10) that drew mercury from the main loop at the upper left and discharged bubbly flow at the lower left. The peristaltic pump was placed in its own secondary container and connected to the main loop via flexible, doubly contained steel reinforced hose. The main flow was circulated clockwise with respect to Figs. 1 and 2 when damage tests were performed.

The loop's right vertical leg was used for strain response investigations. This leg had no features or interfaces in order to provide clean structural conditions to ease strain response interpretation and modeling work. The main flow was circulated counter clockwise for strain tests.

The DTS were made of type 316L stainless steel and were designed so that their test surfaces were flush with the interior walls of the loop; an example is shown in Fig. 3. The material was fully annealed to maximize damage sensitivity to varying test conditions. Test surfaces were carefully polished, micro indented to establish a 5×5 array of fiducial marks (spaced 4 mm apart) and inspected for flaws before irradiation using a scanning electron microscope (SEM, Phillips XL30). Two specimens were employed from each test condition: one at beam entrance and at beam exit.

A single bubble generator was incorporated into the IBBTL. This was a jet type generator that mixes gas at the discharge of a high speed mercury jet flow. A drawing is shown in Fig. 4. While the mercury flow rate through the

Fig. 3. Damage test specimen showing polished test surface.

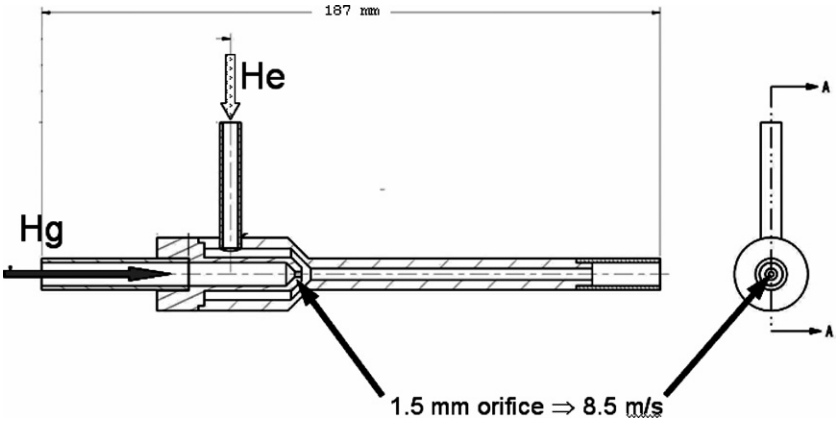

Fig. 4. Jet type mercury – gas bubble generator.

bubbler was low the pressure required to force the fluid through the 1.5 mm diameter orifice was about 500 kPa.

Considerable time was spent at ORNL operating the loop and bubbler prior to irradiation at the WNR. Instrumentation and controls were configured and tested; DTS exchange procedures were practiced through the secondary container glove ports; parameters for optimum bubble generation were developed. Optimization of the exchange procedure reduced the DTS change out time to less than 5 min; this helped reduce radiation exposure to experimenters during the WNR testing.

Two pairs of acoustic hydrophones (Imasonic 0.5 MHz) were used in various combinations with: a lock-in amplifier (Stanford Research SR830); a signal generator/pre-amplifier (Stanford Research DS345 & SR560)/digital oscilloscope (Yokogawa DL708) combination; a device known as an Acoustic Bubble Spectrometer (ABS, Dynaflow, Inc.). The ABS was originally designed for water applications to provide the type of bubble population data of interest here. It had been used previously by ORNL, but its credibility in mercury–bubble mixtures was questionable. The lock-in amplifier was typically used with a continuous 100 kHz signal and would give good measure of the change in attenuation of the transmitted sound with the introduction of gas bubbles. Attenuation of about 1000 times could be achieved with the bubbler operating. The signal generator was programmed to send bursts of sine waves at frequencies from 100 to 600 kHz. At frequencies of 400 kHz and below the bubbles reduced the transmitted signal such that it could not be distinguished from noise; above 400 kHz the attenuation was about 2–1/2 orders in magnitude. While maximizing attenuation helped establish bubbler operating parameters, it did not provide bubble size and void fraction data.

The WNR proton beam pulse parameters used for IBBTL testing included an energy level of 800 MeV, typically 2.5×10^{13} protons per pulse, circular Gaussian profile with $\sigma_R = 9$ mm, and pulse length of 270 ns. Beam position and profile for each pulse were monitored and recorded with an ORNL-developed diagnostic that analyzed video of a fluorescing alumina screen placed in front of and aligned with the target center; beam charge was measured with a current transformer at the end of the beam line. The profile diagnostic assumes bi-directional Gaussian shape, which past experience has been shown to be representative.

The experiment plan was to irradiate a pair of DTS with 100 pulses for each of the three mercury hydrodynamic conditions at a pulse rate of 2 per minute. At least a one hour delay before changing the DTS was allowed to permit radioactivity to subside. The secondary container was not opened for these tasks; new and used DTS were stored inside and were accessed via glove ports.

Loop wall strain response sensitivity to the different mercury conditions was investigated with the beam on spot #2. A fiber optic based system for measuring strain that had been used previously for proton beam experiments was employed [5,13,14]. A total of eight fiber optic strain sensors (FISO FOS) were attached to the loop at the locations shown in Fig. 5. Dynamic responses were obtained with the associated signal processor (FISO Veloce), recorded with digital oscilloscopes (Yokogawa DL 708 and DL716) and a PC based data logger. The recorded time of responses varied from 2 to 50 ms; longer data capture sacrificed some temporal resolution but showed more of the structure's total response to the beam induced pressure. Pulses were applied on demand until adequate strain data was recorded for each mercury condition (roughly 25 pulses).

Experiment collaborators from the JSNS brought their experience and equipment to this test to obtain acoustic emission data associated with cavitation intensity and as well as structural response data from the beam induces pressure pulse. Using a laser Doppler vibrometer (LDV, Ono Sokki LV-1720) the normal velocity of a point on the target loop exterior surface was tracked at a high sampling rate; in this case the laser spot was aimed at a location on the side of the IBBTL leg between the DTS flanges (Fig. 6). The response was filtered either above or below 15 kHz and processed. Localized impacts from cavitation

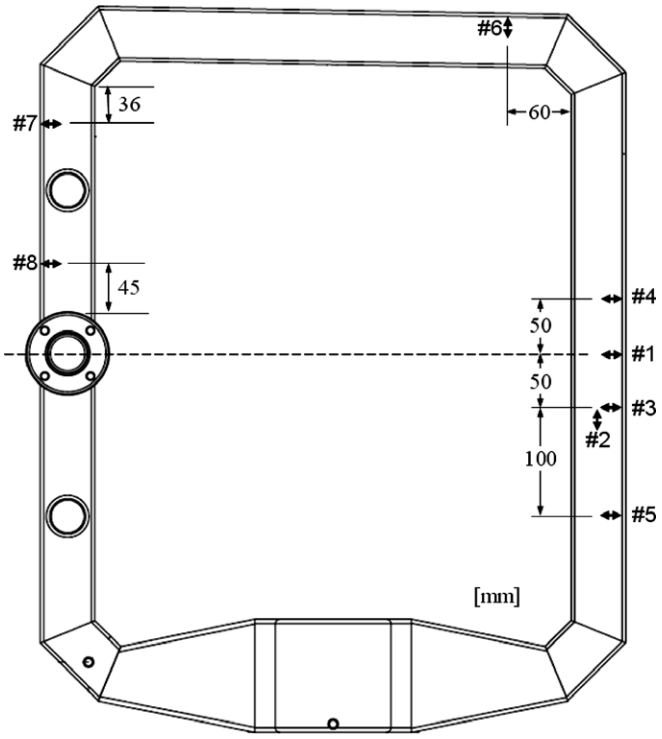

Fig. 5. IBBTL strain sensor layout.

Fig. 6. IBBTL location monitored by LDV.

bubble collapse produce high frequency sound emissions that have been correlated with cavitation intensity [10,11]. The low frequency component of the data is another measure of the target structural response.

A minor test objective was to attempt visual observation of cavitation effects at the beam spot with a transparent sapphire beam window in place of a DTS. The viewing objective was located close to the window and connected to a shielded charge-coupled device camera by ca. 2 m of fiber optic cable.

3. IBBTL results

Damage specimens were removed from the secondary container at the end of irradiation and shipped to ORNL for decontamination and surface analysis. The decontamination procedure has been described elsewhere [5]. Images at each micro indent location were taken with the same SEM used for pre-test inspection at both 100 and 400 times magnification. Fig. 7 shows the worst damage result images for each test condition; a typical pre-test image is also given (a) for reference. The fraction of area damaged is summarized in Table 2 for each mercury test condition along with mean depth of erosion data. This assessment process has also been described previously [4]. The worst damage values determined from all analyzed images are listed.

The stagnant mercury condition clearly incurred the most damage. A notable reduction resulted with mercury flow turned on. The damage was further reduced when bubbles were added to the flow, but the change relative to flow alone was not as large as between flow and stagnant. Bubbles with flow reduced the MDE to one-fourth that of the stagnant condition, which is the same result as the 2002 test.

Processed velocity data obtained by LDV are also given in Table 2. The damage potential parameter E_H was obtained from the high frequency component (above 15 kHz) of velocity; these acoustic emissions are a product of the localized impacts caused by cavitation induced micro-bubble collapse which leads to pitting damage [11,12,15]. The filtered velocity (V_i) is squared at each time point and summed over the response history:

$$E_H = \sum_i^n |V_i|^2. \quad (1)$$

The reported *normalized* E_H values in Table 2 are averages from the 100 pulses used for each test condition; they are normalized to the stagnant result. The trend in E_H with test condition is similar the trends for fraction of damaged area or mean depth of erosion.

E_L is a structural response parameter and is an integrated measure of the response of the loop to the beam induced pressure pulse. It is similarly processed from velocity data but instead uses components below 15 kHz. Ideally E_L would be compared to strains near the LDV spot location, but unfortunately the strain sensor near this (sensor #8) did not track well when the beam was applied at beam spot #1. E_L values suggest a reduced structural response with bubbles injected compared to stagnant mercury, but an increased response with mercury flow without bubbles is also indicated.

Example strain data is shown in Fig. 8 for locations close to (sensors #2 and #4) and distant from (sensor #6) the beam spot for each mercury test condition when beam

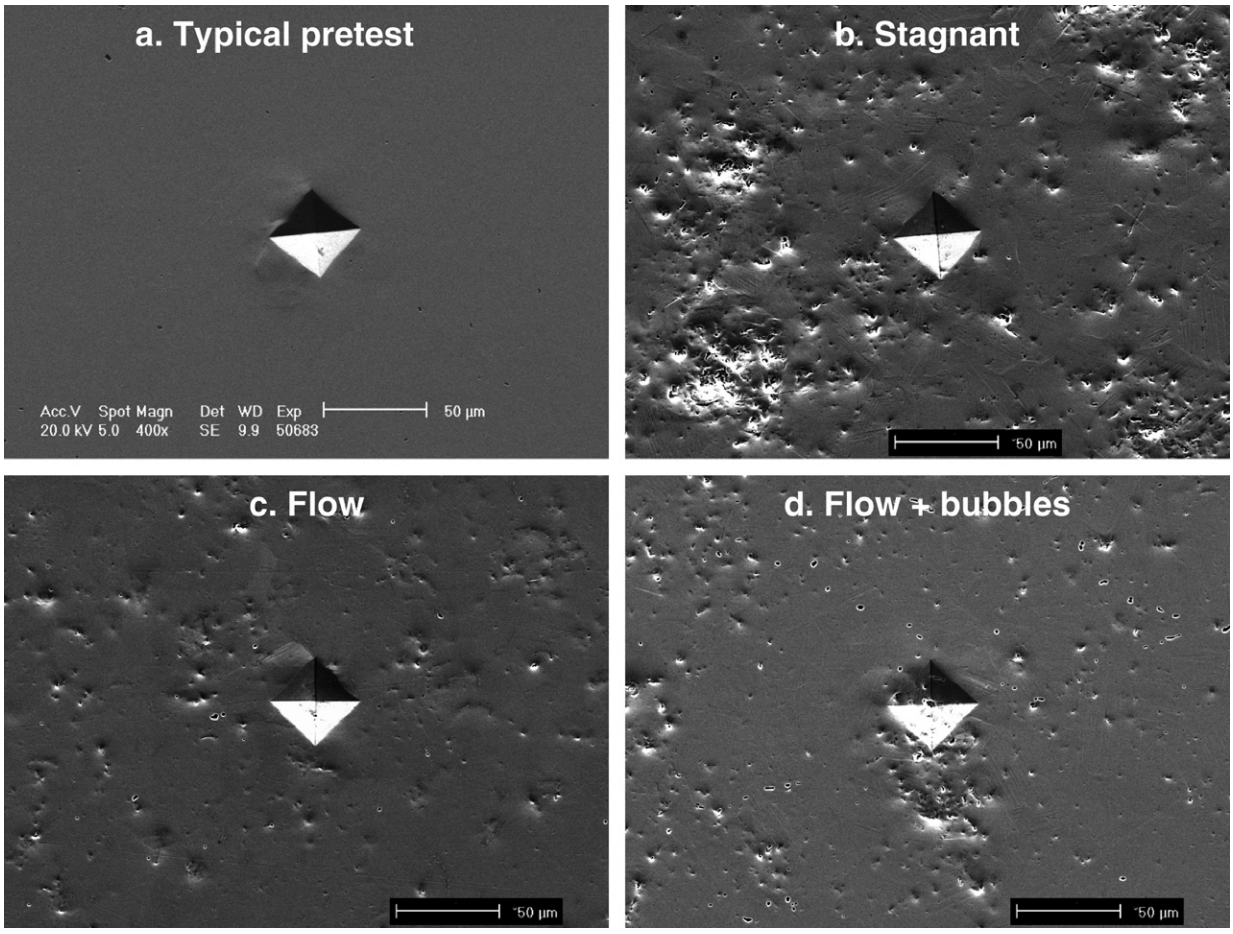

Fig. 7. SEM images from IBBTL damage test.

Table 2
IBBTL damage summary and LDV data

Test condition	Area fraction with pits	MDE[a] (nm)	Normalized E_H value[b]	Normalized E_L value[c]
Stagnant	0.100	240	1.00	1.00
Flowing	0.065	89	0.50	1.20
Flowing with bubbles	0.051	58	0.35	0.40

[a] Mean depth of erosion.
[b] Damage potential parameter.
[c] Structural response parameter.

was applied at spot #2. Strains near the beam spot show the least difference between stagnant, flow, and flow with bubbles. Stagnant and flow conditions resulted in nearly identical strain near the beam spot for the first 2 ms. The introduction of bubbles reduced strain to some extent at these locations. At sensor #2 (Fig. 8(a)), the magnitude of the first minimum is reduced by roughly one-third, although the maximum at 1.3 ms is hardly changed. The reduction at sensor #4 (Fig. 8(b)) is notable but still small. On the other hand, strain sensor #6 (Fig. 8(c)) shows more pronounced reduction with the introduction of bubbles.

No usable result was obtained from visual observation at the beam spot with a transparent sapphire beam window. Due to limited time and resources, less than ideal equipment was used; in particular the desired radiation damage resistant fiber was not obtained. After three beam pulses the received image was completely degraded due to the radiation damaged fiber.

4. Beam intensity experiment description

Three rectangular targets filled with stagnant mercury were employed for this experiment. The design was identical to the basic target used in 2002 WNR tests [4]; an example is shown in Fig. 9. The front and rear plates (beam entrance and exit) were made of type 316L stainless steel. The material was first annealed to establish a baseline condition. Cold rolling (20% thickness reduction) was performed to work harden the material which increases damage resistance [16]. The plates were then machined flat to 2 mm thickness. An insert plate at the bottom of the target (Fig. 9(b)) mocked up a narrow channel feature of the SNS target that guides mercury flow to cool the target beam window. Test surfaces were polished, marked with a 5×5 array of micro indents (5 mm spacing) and pre-inspected at each location at 100 and 400 times magnification.

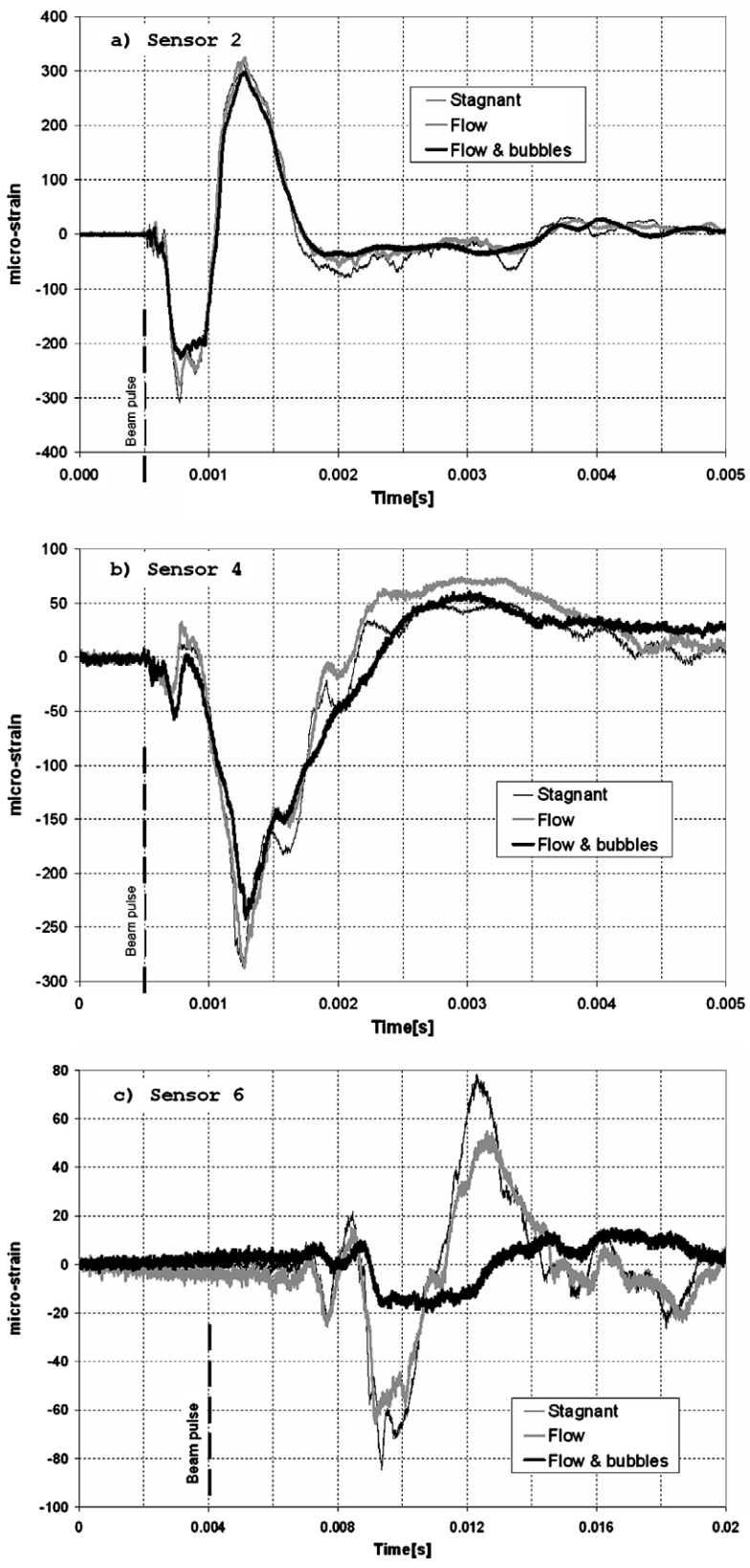

Fig. 8. IBBTL strain examples obtained when the beam was located at spot #2.

Proton energy and number per pulse were kept constant for each test condition (800 MeV, 2.6×10^{13} protons/pulse) but beam size was varied. The intent was to consistently apply elliptic profiles with width (σ_X) three times as large as height (σ_Y). The largest beam size was chosen to completely fill the front plate and the smallest was that

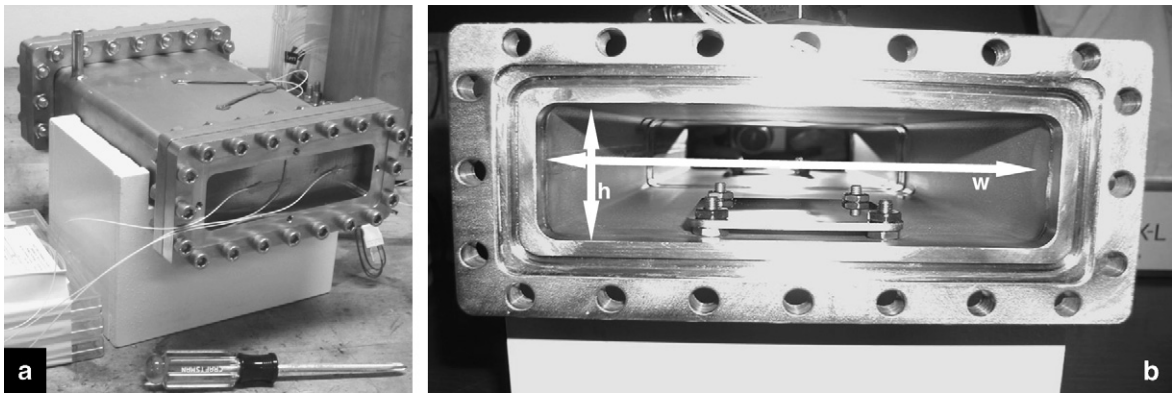

Fig. 9. (a) Rectangular-shaped target used for beam intensity testing. The end plates were 2 mm thick stainless steel (type 316, 20% cold worked). (b) Rectangular target with the front plate removed and showing the insert plate that mocks up a narrow channel feature of the SNS target. Internal dimensions were 41 × 143 × 215 mm ($h \times w \times d$).

which could be focused at this WNR location. An intermediate size roughly split these extremes. In this way the total energy deposited for each condition was the same (ca. 2 kJ/pulse). Conditions were designated Low Intensity (LI), Nominal Intensity (NI) and High Intensity (HI) to indicate relative maximum imparted proton density. One hundred pulses were applied to each test target at a rate of two pulses per minute. Copper foils were installed over and aligned to the front plate of each target to provide a post irradiation integrated measure of incident protons in addition to the real time per pulse beam characterization obtained from the fluorescing screen analysis.

5. Beam intensity experiment damage results

Average beam size, location on target, protons per pulse and maximum proton intensities obtained from the fluorescing screen are summarized in Table 3 from images for each condition. Post irradiation analysis of the copper foils was performed at ORNL in order to provide some confirmatory data for the screen data. The foils were carefully segmented and the pieces around the beam center were measured for the presence of ^{57}Co which is formed only from proton interaction with copper. The activity map was then fitted to Gaussian parameters which are summarized in Table 4 and can be compared to the fluorescing screen data. The agreement is generally good for maximum intensity, protons per pulse, and beam spot size, but beam center locations do not compare as well. The segmentation of the foil may have been too coarse to accurately locate beam profile, but the true cause for the discrepancy is not known.

The surfaces analyzed for damage included the front plate where the beam passed through, the bottom of the insert plate (which faces the narrow mercury channel), and the top of the insert plate (facing the bulk volume of mercury). Worst damage images of the front plate are shown in Fig. 10(a)–(c) and damage data is summarized in Table 5. Surprisingly, the nominal intensity case exhibited the least damage.

Bottom surface insert plate damage was notably larger than the front plate, which is consistent with previous experience. This plate was essentially out of the proton beam path so correlating with intensity might seem inappropri-

Table 3
Intensity test beam parameters from video analysis of fluorescing screen

Intensity	σ_X (mm)	σ_Y (mm)	X-Center (mm)	Y-Center (mm)	Protons/pulse ($\times 10^{12}$)	Maximum intensity (p/mm^2 $\times 10^{10}$)
HI	13.68	4.26	−0.10	−0.77	26.8	7.34
NI	25.12	7.00	0.98	3.17	26.4	2.39
LI	30.87	10.96	1.47	1.22	25.6	1.21

Averages of 100 pulses for each condition are shown.

Table 4
Intensity test beam parameters from copper foil analysis

Intensity	σ_X (mm)	σ_Y (mm)	X-Center (mm)	Y-Center (mm)	Protons/pulse ($\times 10^{12}$)	Maximum intensity (p/mm^2 $\times 10^{10}$)
HI	11.47	5.99	1.89	8.89	28.4	6.56
NI	25.82	7.51	5.44	−1.26	31.6	2.59
LI	35.25	10.92	−1.00	0.32	30.4	1.26

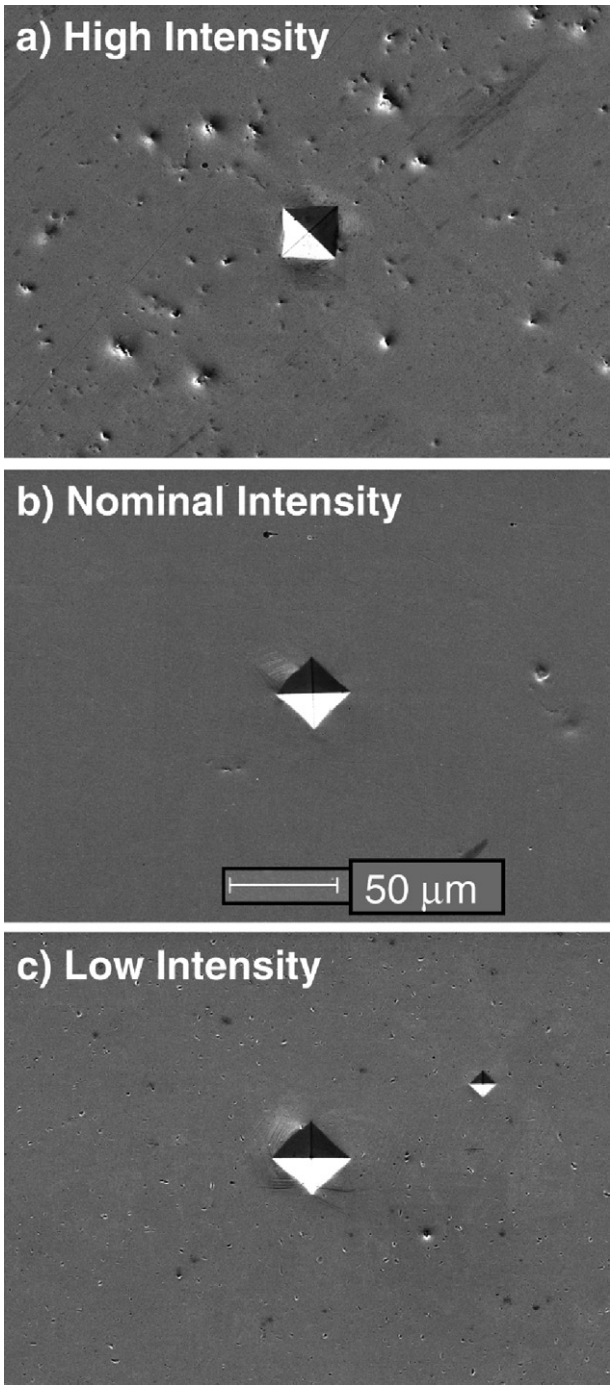

Fig. 10. Front plate damage from beam intensity test. These are worst damage images originally taken at 400×. Note that (c) has an improperly placed small indent that has been discounted in the damage analysis.

ate. Nevertheless, the insert plate bottom surface damage trend is essentially linear with proton intensity. An example image is shown in Fig. 11 with several large pits.

6. Discussion

Despite the effort put into the IBBTL test apparatus design and more thorough pre-beam testing, the achieved degree of damage mitigation with bubble injection was only a factor of 4 compared to stagnant mercury. This is the same degree that was achieved in the 2002 bubble test. This still falls short of intentions for a mitigation technique to be incorporated into the SNS. A continued frustration was the inability to quantify the established bubble population even though significant acoustic attenuation was measured. The relationship between actual bubble population and theoretical requirements for effective mitigation could not be determined. Improvements in bubble diagnostics remain a key element to the SNS Target R&D program. The pace of small gas bubble generation in mercury technology will be slowed without credible diagnostics.

The reduction in damage due to mercury flow alone is a positive finding. The region of mercury flow dedicated to cooling the SNS target window is of particular concern for cavitation damage based upon target tests that included a mock up of the region. However, those experiments had stagnant mercury whereas in the SNS the velocity will range from roughly 1–3.5 m/s. The IBBTL results suggests that the vulnerability may not be as severe as previously thought. The degree of mitigation that might be expected at SNS velocities (vs. the 0.4 m/s in the IBBTL) is to be investigated in a future in-beam target test. Further, it is noted that there was no significant mercury flow in the 2002 WNR bubble test where damage with bubbles was about one-fourth that without bubbles. Having achieved about the same damage reduction in 2005 with combined

Table 5
2005 Intensity test damage summary

Test condition	Front plate		Insert plate, surface facing bulk Hg (top)		Insert plate, surface facing Hg slot (bottom)	
	Fraction of area with pits	MDE (nm)	Fraction of area with pits	MDE (nm)	Fraction of area with pits	MDE (nm)
HI	0.030	37	0.048	128	0.120	1400
NI	0.0096	14	0.0026	3.4	0.038	270
LI	0.015	19	0.006	6.8	0.012	26

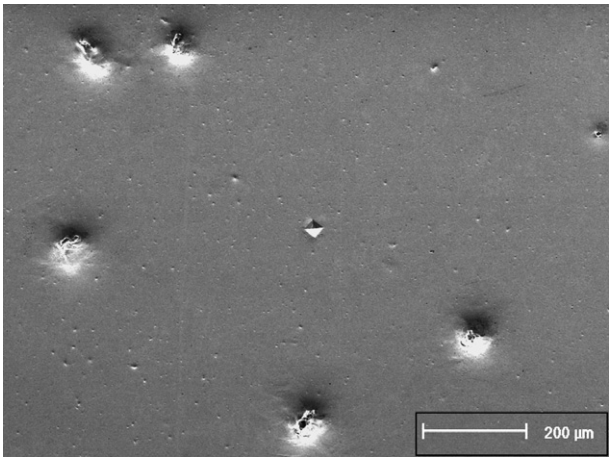

Fig. 11. Image from bottom surface of HI insert plate.

flow and bubbles might suggest that the earlier bubble generation was better than achieved in 2005.

During exploration of IBBTL bubble generator parameters [9], most attention was paid to attenuation of sound between the hydrophones that was being either continuously transmitted with the lock-in amplifier or intermittently with sine bursts from the signal generator. More review of the sine burst data for effects of sound speed changes has since been performed. It has been noted that the delay between sent and received signals when the bubbler was turned on was consistent with mercury's nominal sound speed (about 15 μs for 22 mm of mercury) and this delay was constant over the 50–600 kHz interrogation range. This was an indication the bubbles were large, that is, their resonant frequency was low relative to burst frequency. Therefore the observed attenuation was due to scatter of the sound wave as opposed to absorption (compression of the bubbles). Scattering would be less useful in reducing the maximum beam induced pressure in the immediate region of the beam spot, but would be helpful in remote regions. This interpretation is consistent with damage and strain observations.

Helium bubbles in mercury with a resonance of 100 kHz are small. Fig. 12 shows the dependence of bubble resonant frequency with size; 100 kHz corresponds to a bubble diameter of about 20 μm, which is desirable but quite small. In hindsight there seems to be less value in probing with frequencies much higher than 100 kHz. Conversely, not having interrogated the bubbly mixture at frequencies below 50 kHz probably missed evidence of larger bubbles. 50 kHz corresponds to a diameter of about 40 μm and it is plausible that mostly bubbles larger than this were generated.

Another point regarding the acoustic interrogation of the bubbly mixture concerns the choice of hydrophones. Dynaflow (who is presently under contract with SNS for bubble diagnostic development) tested the frequency response of a pair of Imasonic 0.5 MHz hydrophones in water after the IBBTL experiment. A good response around 0.5 MHz and down to 200 kHz was confirmed but below this the response falls sharply. At 100 kHz and below received signals were barely detectable above noise levels in the Dynaflow test. This deficiency would be similarly applicable when the hydrophones were used in mercury; it is now clear that this model of hydrophone was not ideally suited to the frequency range or bubble sizes of interest.

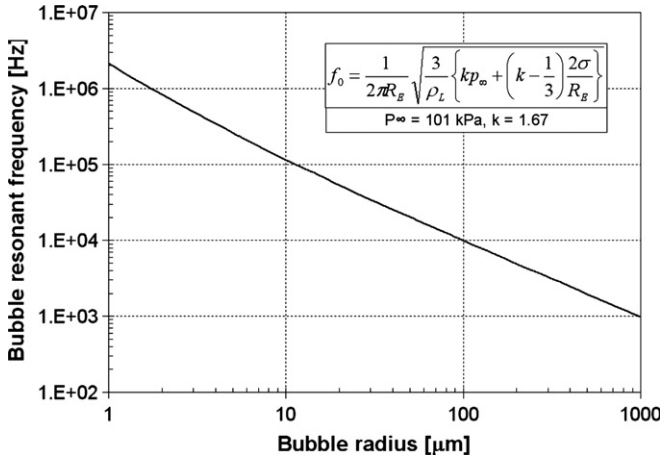

Fig. 12. An example of helium bubble in mercury resonance dependence on size. Adiabatic conditions are assumed.

The strain data obtained from IBBTL has contributed to the understanding of the structural response of mercury filled vessels hit with short and intense proton beam pulses. For example, one might expect that stress wave propagation in the steel leg from beam spot #2 up to sensor #6 (Fig. 8(c)) should arrive about 70 μs after the pulse. The distance is about 0.33 m and the speed of sound in steel is about 4500 m/s. However, no significant strain was observed at this time. If mercury's sound speed (1500 m/s) was applicable then a response would be seen about 210 μs; in fact the major response of sensor #6 did not begin until nearly 3 ms after the pulse. As has been seen in previous mercury target tests [14,17] the time responses of the most significant strains are often longer than wave transport times. These strains are characteristic of the structural dynamics of the liquid filled target; these are a function of system stiffness and mass. In particular, the time for the response to reach sensor #6 is greatly influenced by the radial compliance of the loop wall.

The introduction of helium bubbles notably reduced strain magnitudes at sensor #6; similar reductions were not observed at sensors #2 and #4 which are close to the beam spot. It is speculated that there were insufficient small bubbles in the direct vicinity of the beam spot to absorb the beam induced pressure in the time scale of the pulse (<1 μs). At distances further away the larger bubbles could absorb the slowly propagating disturbance, scatter the pressure wave, or some combination of these mechanisms. The strain response and pressure wave propagation in the IBBTL was investigated further in Ref. [18].

The correlation of the damage potential parameter E_H with observed damage is an important validation of the acoustic emission technique for estimating cavitation intensity driven by short pulse proton irradiation. This was not obvious at the time of the bubble injection test; the reduction in the apparent velocity peaks was irregular with each beam pulse. At the time it was speculated that the bubble population was not steady due to the surging nature of the peristaltic pump pressure discharge, but review of its output pressure history and pulse timing failed to provide corroboration. In any case, the average normalized E_H data correlates with the observed damage reduction. The implication is that the technique will be useful in evaluating mitigation technologies and it will reduce the need for evaluation of actual cavitation damage.

With regard to the low frequency component of LDV data, it is argued [11] that E_L is proportional to the peak pressure caused by the proton beam and thus should corre-

Table 6
2002 Intensity test damage summary, front plate

Test condition	Fraction of area with pits	MDE (nm)	Protons/pulse[a] ($\times 10^{12}$)	Maximum intensity [a] ($p/mm^2 \times 10^{10}$)
TL – 'high power'	0.046	132	27.7	3.63
TM – 'medium power'	0.003	12	15.1	1.59
TH – 'low power'	0.002	4	2.8	0.58

[a] Average of fluorescing screen data.

late with strain response. The E_L value for the flow with bubbles condition is notably less than for the stagnant condition. This is consistent with stain data at sensor #6 (taken with the beam at spot #2) but not with strain data near the beam spot. The increase in E_L with flow alone is difficult to understand. It had been visually observed that the loop moves slightly and at low frequency when the main flow pump is operating. Such motion induced strains barely measurable by the strain sensors, but the LDV may have been more sensitive to it. This motion may be the origin of the higher value of E_L for flow without bubbles.

The results from the beam intensity experiment have raised a number of questions. The trend in MDE with proton intensity clearly does not support a power law dependency. In addition, when these results are compared to 2002 intensity results they are inconsistent. Table 6 shows 2002 pitting damage data (from Ref. [4]) along with corresponding beam parameters. The 2002 case 'TL' had comparable total protons and intensity (fluorescent screen data) compared to the 2005 NI case, yet NI has about one-tenth of the MDE of TL. Additional SEM images were taken of the NI front plate away from any indents where somewhat greater damage was found, but this damage was still considerably less than the 2002 TL case. Further, the 2005 HI case had greater intensity than TL yet it still had less than one-third of TL's MDE. The front plates used in 2005 were unused pieces from the 2002 experiment and have the same material pedigree. Comparison of indent sizes on SEM images (made under the same load) verified the same hardness levels in 2002 and 2005 plates. As best as can be determined, all test conditions were essentially the same. An explanation has yet to be found.

7. Conclusions

In-beam experiments investigating cavitation damage in short pulse mercury spallation targets were carried out at the WNR facility in LANSCE in 2005. Two types of test targets were used. The first was a small mercury loop that could circulate mercury and incorporate small gas bubble injection as a means to mitigate damage. Tests with the loop included a baseline case with stagnant mercury, a case with mercury flowing but without bubbles, and a case with bubbles injected into the mercury flow. Flow alone reduced damage to less than half that of stagnant mercury. The bubble condition reduced damage by four times compared to stagnant mercury. This was disappointing and no further improvement over a simpler in-beam test done in 2002. Continued problems with diagnostics to determine the generated bubble population made establishing more favorable conditions difficult. Laser Doppler vibrometer data was obtained for all three mercury conditions that were processed to give measures of cavitation damage potential. The potential data has shown correlation to the observed damage thus helping validate the technique's usefulness for off-line development of damage mitigation technology. Some interesting data was obtained on loop strain response to the beam induced pressure pulse. Overall, indications were that the established bubble population was comprised of bubbles too large in size to sufficiently mitigate the pressure wave and cavitation damage.

The second type of test target was a rectangular-shaped vessel filled with stagnant mercury. Three such targets were irradiated with 100 pulses of the same number of protons but with different beam profiles. The goal was to vary proton intensity while maintaining constant energy deposited in the targets. While previous in-beam tests, off-line experiments, and theory have indicated cavitation erosion rate to be in proportion to the intensity raised to the fourth power, the results from this test did not support such a dependency. Damage results at the front plate of the targets (where the beam passes through) were hard to understand. For example, the intermediate intensity produced slightly less damage than the lowest intensity, and all damage results are low relative to comparable intensity tests done in 2002. However, it was observed that damage on a surface that faced a narrow mercury slot and was outside the proton beam correlated linearly with proton intensity.

Acknowledgments

The authors extend their gratitude to supporting WNR experimenters Bobby Cross, Duncan Earl, Dave Felde, Phil Ferguson, Bob Sangrey and Jim Tsai. The support of LANSCE operations, safety and radiological staff were greatly appreciated as well as the technical assistance at the WNR from Gregg Chaparro, Bruce Takala and Steve Wender. David Glasgow is to be credited with ^{57}Co counting of copper foils and Tom McManamy for analysis of that data.

This work has benefited from the use of the Los Alamos Neutron Science Center at the Los Alamos National Laboratory. This facility is funded by the US Department of Energy.

References

[1] T.E. Mason, T.A. Gabriel, R.K. Crawford, K.W. Herwig, F. Klose, J.F. Ankner, in: 20th International Linac Conference, 21–25 August 2000, Monterey, California, Published on the LANL Print Server, <http://xxx.lanl.gov/>.
[2] T.A. Gabriel et al., J. Nucl. Mater. 318 (2003) 1.

[3] K. Haga, H. Kogawa, H. Satoh, S. Ishikura, H. Kinoshita, M. Futakawa, M. Kaminaga, in: Proceedings of the 17th Meeting of the International Collaboration on Advanced Neutron Sources (ICANS-XVII), April 2005.
[4] J.R. Haines, B.W. Riemer, D.K. Felde, J.D. Hunn, S.J. Pawel, J. Nucl. Mater. 343 (2005) 58.
[5] B.W. Riemer, J.R. Haines, J.D. Hunn, D.C. Lousteau, T.J. McManamy, C.C. Tsai, J. Nucl. Mater. 318 (2003) 92.
[6] J.D. Hunn, B.W. Riemer, C.C. Tsai, J. Nucl. Mater. 318 (2003) 102.
[7] H. Soltner, Gas Bubble Admixture for Pressure Pulse Mitigation in High-power Liquid–Mercury Spallation Targets, ESS 03-152-T, Forschungszentrum Jülich, 2003.
[8] H. Soltner, Effects of Gas Bubble Admixture on Pressure Pulse Propagation in Liquids, ESS 03-153-T, Forschungszentrum Jülich, 2003.
[9] M.W. Wendel, B.W. Riemer, J.R. Haines, in: Proceedings of the 17th Meeting of the International Collaboration on Advanced Neutron Sources (ICANS-XVII), April 2005.
[10] M. Futakawa, T. Naoe, C.C. Tsai, H. Kogawa, S. Ishikura, in: Proceedings of the Fifth International Symposium on Cavitation (CAV2003), 2003.
[11] M. Futakawa, H. Kogawa, S. Hasegawa, Y. Ikeda, B. Riemer, M. Wendel, J. Haines, G. Bauer, T. Naoe, N. Tanaka, K. Okita, A. Fujiwara, in: Proceedings of the Sixth International Symposium on Cavitation (CAV2006), 2006.
[12] H. Kogawa, S. Hasegawa, M. Futakawa, Y. Ikeda, B. Riemer, M. Wendel, J. Haines, in: Proceedings of the 17th Meeting of the International Collaboration on Advanced Neutron Sources (ICANS-XVII), April 2005.
[13] J.R. Haines, B.W. Riemer, D.K. Felde, J.D. Hunn, M.W. Wendel, Final Report on Mercury Target Development, ORNL/SNS 101050000-TR0001-R00, 2003.
[14] M.R. Cates, Strain Measurements On Targets Tested at the LANSCE – WNR Facility August 2000, ORNL/SNS 101050200-TR0009-R00, July 2001.
[15] H. Soyama, M. Futakawa, in: Proceedings of the Fifth International Symposium on Cavitation (CAV2003).
[16] S.J. Pawel, E.T. Manneschmidt, J. Nucl. Mater. 318 (2003) 122.
[17] B.W. Riemer, J. Nucl. Mater. 343 (2005) 81.
[18] H. Kogawa, these Proceedings.